Thermal-Induced Dissociation and Unfolding of Homodimeric DsbC Revealed by Temperature-Jump Time-Resolved Infrared Spectra

Heng Li,[†¶] Huimin Ke,[‡¶] Guoping Ren,[§] Xianggang Qiu,[†] Yu-Xiang Weng,[†*] and Chih-Chen Wang[‡*]
[†]Laboratory of Soft Matter Physics, Institute of Physics, Chinese Academy of Sciences, Beijing, China; [‡]National Laboratory of Biomacromolecules, Institute of Biophysics, Chinese Academy of Sciences, Beijing, China; [§]Howard Hughes Medical Institute, Department of Molecular, Cellular and Developmental Biology, University of Michigan, Ann Arbor, Michigan; and [¶]Graduate School of the Chinese Academy of Sciences, Beijing, China

ABSTRACT The thermal stability of DsbC, a homodimeric protein disulfide isomerase in prokaryotic periplasm, has been studied by using temperature-dependent Fourier transformation infrared and time-resolved infrared spectroscopy coupled with temperature-jump initiation. The infrared absorbance thermal titration curves for thermal-induced unfolding of DsbC in D_2O exhibit a three-state transition with the first transition midpoint temperature at 37.1 $\pm$ 1.1°C corresponding to dissociation, and the second at >74.5°C corresponding to global unfolding and aggregation. The dissociation midpoint temperature of DsbC in phosphate buffer shifts to 49.2 $\pm$ 0.7°C. Temperature-jump time-resolved infrared spectra in D_2O shows that DsbC dissociates into the corresponding germinate monomeric encounter pair with a time constant of 40 $\pm$ 10 ns independent of the protein concentration and 77% of the newly formed monomeric encounter pair undergoes further coil to helix/loop transition with a time constant of 160 $\pm$ 10 ns. The encounter pair is expected to proceed with further dissociation into monomers. The dissociation of DsbC is confirmed by size-exclusion chromatography and subunit hybridization. The in vivo oxidase activity of DsbC attributed to the monomer has also been observed by using cadmium sensitivity and the oxidative state of β-lactamase.

INTRODUCTION

Disulfide bonds are important for the folding, stability, and function of many proteins. In prokaryotic cells they are catalytically formed by the Dsb family proteins in the periplasm (1). The DsbA rapidly donates its disulfide bond to unfolded secreted or membrane proteins, and is then reoxidized by an inner membrane protein DsbB, constituting the oxidation pathway (1). The disulfide isomerase DsbC, composed of 2 $\times$ 216 amino acid residues (2) with chaperone activity (3), is thought to isomerize mismatched disulfide bonds and to be kept reduced by another inner membrane protein DsbD (1), constituting the reduction/isomerization pathway. It has been shown recently that DsbC can also assist DsbA to oxidatively fold envelope proteins in a DsbD-independent manner, which suggests that some cross talk can occur between the two pathways (4).

The disulfide isomerase DsbC is a V-shaped homodimer with each arm of the V as a subunit, which consists of the N-terminal domain responsible for dimerization connected via a hinged linker helix to the C-terminal thioredoxin (Trx)-fold domain (5). The two active sites (Cys^{98}-Gly-Tyr-Cys^{101}), one in each Trx-fold domain, are essential for isomerase activity. Linkage of monomeric Trx, DsbA or the *a* domain of protein disulfide isomerase, each of which individually has no or low isomerase activity, to the association domain of DsbC, forms a dimeric molecule, which acquires isomerase activity (6). Substitution of $glycine^{49}$ (Gly^{49}) with arginine (Arg) converts the dimeric disulfide isomerase into a monomeric oxidase (7,8), suggesting that dimerization acts to protect DsbC active sites from DsbB-mediated oxidation (7,9,10). By comparative study of the intrinsic fluorescence changes of DsbC and its two mutants DsbC-G49R and Y52W with excitation at both 295 and 280 nm, Ke et al. (8) have shown that guanidine hydrochloride (GdnHCl)-induced unfolding of dimeric DsbC is a thermodynamically reversible three-state transition via a stable monomeric folding intermediate formed in the first transition at low GdnHCl concentrations.

The temperature-jump (T-jump) technique provides a unique means to study the thermal stability of proteins by triggering a fast protein unfolding/folding process with a heat pulse at an accessible temporal resolution as high as 70 ps (11). Fourier transform infrared (FTIR) absorption in the amide I band for polypeptides provides finger prints of the secondary structures (12–14). A combination of the T-jump and the time-resolved infrared (IR) absorbance difference spectra has become a powerful tool for tracing the changes of secondary structures in the thermal-induced folding/unfolding dynamics of proteins (15,16). By using these methods we have investigated the thermal stability of the DsbC dimer, which, to the best of our knowledge, has not been studied before. Our results show that the DsbC dimer undergoes thermal-induced dissociation at a midpoint temperature (T_m) of 37.1°C in D_2O and 49.2°C in phosphate

Submitted April 8, 2009, and accepted for publication August 27, 2009.

Heng Li and Huimin Ke contributed equally to this work.

*Correspondence: yxweng@aphy.iphy.ac.cn or chihwang@sun5.ibp.ac.cn

Editor: Feng Gai.

0006-3495/09/11/2811/9 $2.00

doi: 10.1016/j.bpj.2009.08.049

D_2O buffer. The DsbC dissociation path revealed by IR studies is further supported by biological evidence.

MATERIALS AND METHODS

Materials

Recombinant DsbC and DsbC-G49R proteins were prepared according to Ke et al. (8) (see the Supporting Material) in 99.9% D_2O (pD 5.8) or D_2O buffer containing 50 mM K_2DPO_4/KD_2PO_4 (pD 7.0) at 12.5 mg/mL. A solution of mixed glutamic acid (Glu) and aspartic acid (Asp) with a weight ratio of 1:2 close to that of the DsbC molecule was prepared in D_2O at 12.5 mg/mL. In addition, DsbC carboxymethylated at both thiols of the active site −CGYC− motif, known as mmDsbC, was prepared according to Zapun et al. (2).

FTIR spectroscopy

Temperature-dependent FTIR spectra were collected on a spectrometer (ABB-BOMEM, Bureau, Quebec, Canada) equipped with a liquid nitrogen cooled broad band mercury-cadmium-telluride detector. A two-compartment CaF_2 sample cell with a 56-μm thick Teflon spacer was used for the protein solution and reference D_2O, respectively. The measurements were carried out in a homemade vacuum chamber with a temperature controlled to an accuracy of $\pm 0.1^\circ$C by water circulation. An average of 50 scans was taken for each spectrum.

T-jump and time-resolved IR difference absorbance spectra

The T-jump IR apparatus has been described in Ye et al. (17) and Zhang et al. (18). Briefly, the 1.9-μm T-jump pulse was generated via Raman shifting the fundamental output of a Nd/YAG laser (Lab 170, 10 Hz, 8–12 ns; Spectra Physics, Mountain View, CA) in a cell filled with 750 psi H_2 gas. The T-jump induced transient IR absorbance changes were measured by using a mid-IR CO laser at a spectral resolution of ≥ 4 cm^{-1} (Dalian University of Technology, Dalian, China), in conjunction with an mercury-cadmium-telluride detector (Kolmar, Newburyport, MA) and a digital oscilloscope (Tektronix model TDS 520D). The temperature-dependent FTIR spectra of D_2O were taken as an internal standard for T-jump calibration (17,19,20). The temporal resolution after deconvolution of the instrumental response of this system is ~30 ns (17). The instrument response function is limited mainly by the detector/preamplifier system. The combined total response function set as Gaussian was determined to be approximately with a bandwidth (full-width at half-maximum) of 80 ns. This experimentally determined instrument response function was convolved with a single exponential to best fit the infrared transient (21,22).

The T-jump time-resolved IR difference absorbance spectrum requires repeated data collection for a high signal/noise ratio, thus the reversibility of the protein folding/unfolding is imperative for reliability of the data. FTIR spectra for heating-and-cooling cycled sample were collected to determine the highest accessible temperature at which reversibility of the protein folding/unfolding remained (17). This was found to be ~40°C and 70°C for DsbC and DsbC-G49R in D_2O, respectively.

Spot titers for cadmium resistance

Spot titers were used to measure the relative cadmium resistance of different genotype strains according to Quan et al. (23). Briefly, mid-log phase cells of different strains with an optical density (OD_{600}) of 1 were serially diluted in sterile 150 mM NaCl. Each dilution of 2 μL was plated onto LB plates supplemented with 0, 5, 10, 20, 40, 100, and 200 μM of $CdCl_2$ and 10 μM IPTG, and incubated overnight at 37°C and 42°C. All spot titers were carried out in duplicate or triplicate.

Oxidation of β-lactamase by DsbC in vivo

Mid-log phase cells containing pBR322 with OD_{600} of 1 at 37°C were collected for resuspension in 5% trichloroacetic acid, and the acid precipitates were alkylated by incubation in 50 mM Tris-HCl, pH 8.0, with 10 mM 4-acetamido-4′-maleimidylstilbene-2,2′-disulfonic acid (AMS), 1 mM EDTA, and 1% SDS for 30 min at 30°C and another 10 min at 37°C. The reactions were analyzed by NUPAGE Tris-Glycine 14% (Invitrogen, Carlsbad, CA). The disulfide bond formation in β-lactamase (Bla) was visualized by Western blot with rabbit anti-Bla antibody (Chemicon, Temecula, CA).

RESULTS AND DISCUSSION

Although DsbC in crystal has been shown to exist as a dimer, the structural elements involved in dimerization are surprisingly small, limited to two pairs of very short β-strands. The dimerization domains are composed of one α-helix (α_1) and six-stranded central β-sheet (β_1–β_6) with the interface formed essentially by only nine β-sheet hydrogen bonds linking β_4 to the β_5 of the opposite monomers (6) (Fig. 1). The interaction, consisting almost entirely of just nine hydrogen-bonds, may be relatively weak, and quite a few single-point mutants result in monomerization of the protein (7). Monomeric DsbC mutant only shows oxidase activity (7,8). Furthermore, DsbC has been reported to show oxidative activity under certain conditions (4). To study the thermal stability of the DsbC dimer, we tried to find spectroscopic tags for dimerization/monomerization using infrared spectroscopy. The amide I band in particular is very sensitive to secondary structural elements and intermolecular hydrogen bonding between $-COO^-$ groups and $-NH_3^+$ groups or solvent H_2O (D_2O) molecules (see Table 1 for the wavenumber assignments of the various spectral bands). We reasoned that comparison of wild-type dimeric DsbC with the single-point mutant DsbC-G49R, which acts to monomerize DsbC, might allow us to find a spectroscopic signal for dimerization. If such a tag-signal could be found we could analyze the kinetics and temperature dependence of the dimer-monomer transition.

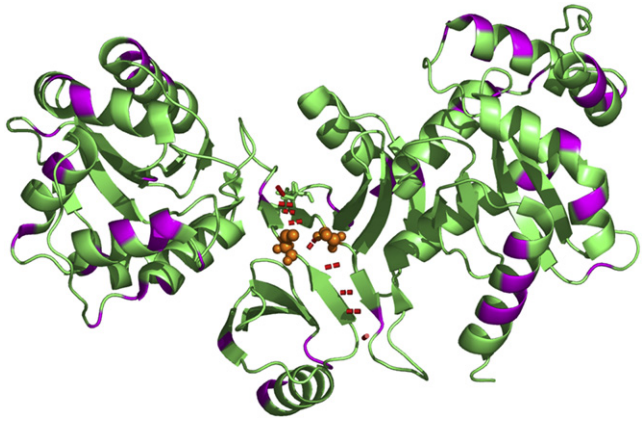

FIGURE 1 Cartoon representation of the crystal structure of dimeric DsbC (Protein Data Bank 1EEJ and PyMOL). The residues of Glu and Asp are shown in pink, Gly^{49} as orange spheres, and the nine hydrogen bonds between the two monomers as red dotted lines.

TABLE 1 Assignment of the observed amide I band

Observed (cm^{-1})			Reported (cm^{-1})	
FTIR	T-jump	Assignment	average/extremes	References
1610	1608	Hydrogen bonding between $-COO^-$ and intermolecular amino acid	1605/1600 ~ 1610	(28,34)
1623	1619	Hydrogen bonding between $-COO^-$ and solvent molecules	1619/1617 ~ 1620	(28,34)
1614	1614 (low-frequency)	Intermolecular anti-parallel β-sheets from aggregation	1620/1610 ~ 1630	(19,34–38)
1681	1684 (high-frequency)		1683/1680 ~ 1690	
1632	1627	β-sheet	1630/1623 ~ 1641	(34,36,39)
1641	1640	Random coil	1645/1640 ~ 1650	(34,36,39)
1654	1650, 1658	α-Helix and loop	1652/1650 ~ 1656	(12,17,27,34,39–41)
	1664, 1674	Turn	1671/1660 ~ 1675	(34,42–44)

Steady-state FTIR spectra at various temperatures

The IR spectra of dimeric DsbC protein (Fig. 2 *A*) and the monomeric DsbC-G49R mutant (Fig. 2 *C*) are broadband spectra, in which the intensities of the main spectral peaks decrease with increasing temperature accompanied by an increase in absorption at flanking wavenumbers. Here, the weight concentrations of the two proteins are the same; however, the observed IR absorption intensities are different. This can be attributed to the electric effect on the dipole moment transition strength (24,25). As the surface of the DsbC molecule becomes charged, the monomeric unit exerts an electric field on its counterpart, leading to an increased IR absorbance with respect to the monomer in a less polar medium D_2O. When the ionic strength of the medium increases as in a buffer solution, the intensity difference between the dimer and the monomer become reversed (data not shown). Second-derivatives of the absorption spectra with an enhanced spectral sensitivity are used to find the component absorption peaks, and that of the background absorption as a reference shows that the peaks in the second derivative spectra of the proteins are indicative of the secondary structural components rather than the noises (Fig. 2, *B* and *D*) (26,27). As shown in Fig. 2 *B*, the second-derivative spectra of DsbC at 25°C exhibit three major troughs at ~1632, 1654, and 1681 cm^{-1} probably due to β-strands, α-helices/loop, and side-chain carboxyl groups, respectively. Remarkable differences are found for these two proteins, i.e., a significant band at 1641 cm^{-1} attributed to random coils appears for DsbC-G49R but is insignificant for DsbC, suggesting that there are more random coils in the former. On heating to 80°C, an increased peak at 1684 cm^{-1} and the appearance of a new trough at 1615 cm^{-1} suggest the formation of anti-parallel β-sheets in both aggregated DsbC and DsbC-G49R. It is notable that the circular dichroism (CD) spectra of DsbC and DsbC-G49R at room temperature are exactly the same (data not shown), incapable of showing any secondary structural difference between the dimer and monomer.

The absorption spectra of DsbC taken at 25°C and 50°C are significantly different (Fig. 2 *A*), but those of DsbC-G49R are basically identical (Fig. 2 *C*). This suggests that dimeric DsbC but not monomeric DsbC-G49R undergoes conformational changes at temperatures between 25°C and 50°C, caused mainly by monomerization.

The DsbC crystal structure shows clearly that there are some β-sheets participating in the formation of dimeric

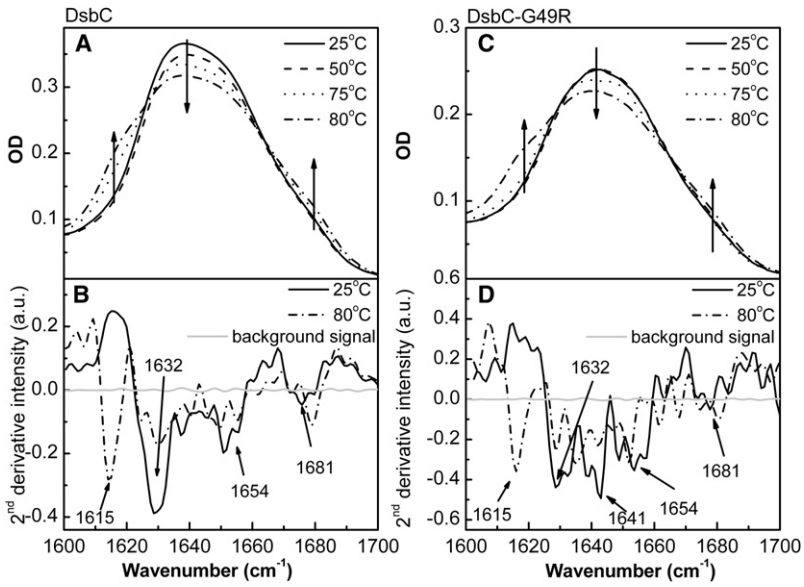

FIGURE 2 FTIR absorption spectra and corresponding secondary derivative spectra for DsbC and DsbC-G49R. (*A*) Absorption spectra of DsbC at 0.2 mM, in D_2O (pD 5.8); (*B*) the corresponding second derivative spectra. (*C*) Absorption spectra of DsbC-G49R at 0.4 mM, in D_2O (pD 5.8); (*D*) the corresponding second derivative spectra. The second derivative of the background absorption (without sample) is plotted for comparison. Experiments were carried out at the temperatures as indicated. Arrows in the absorption spectra denote the direction of the absorbance change with increasing temperature.

interface, and thus the signal around 1630 cm^{-1} is a particularly sensitive measure of the dimer formation. The thermal titration curve of DsbC at 1629.5 cm^{-1} exhibits a three-state transition curve with the first transition midpoint temperature (T_m) at 37.1 ± 1.1°C and the second deduced to be >74.5°C (Fig. 3 *A*), where the uncertainty is caused by lack of a clearly defined upper plateau. In contrast, the IR absorbance thermal titration curve for DsbC-G49R at 1638 cm^{-1} only shows a two-state transition with T_m> 83.8°C (Fig. 3 *B*). In fact, the thermal titration curves at other wavenumbers all exhibit a roughly two-state transition. Because the first transition is absent from the monomeric mutant, we ascribe the transition with $T_m = 37.1 \pm 1.1$°C to the disruption of the β-sheets participating in dimerization. It should be noted that for DsbC, when the temperature is raised from 10°C to 30°C, the slight increase in the IR absorbance of the dimer and monomer does not correspond to the secondary structural change, but is probably due to the salt effect on IR absorption in the buffer, which results from thermally activated ions binding onto the hydrophobic surface. In D_2O, the ions are protons.

Besides the secondary structure, hydrogen bonding near the dimeric interface can also be a good indicator of dimerization. The absorption band at 1619 cm^{-1} can be assigned to asymmetric stretching of side-chain carboxylate groups of Asp or Glu residues forming hydrogen bonds with water molecules (28). After the thermal titration of DsbC at 1619 cm^{-1} two transitions are also found with one having a T_m at 36.0 ± 1.0°C and another at >74.6°C (Fig. 3 *C*). In contrast, DsbC-G49R at this wavenumber again shows only a single transition starting around 72°C. The minor change in the thermal titration curve for DsbC-G49R at temperatures below 55°C closely parallels that of free Glu/Asp acids in solution, suggesting that it is not specific to the thermal-induced protein conformational change. Thus the transition observed with a T_m of 36.0 ± 1.0°C reflects the opening of the hydrophobic clefts during the thermal disruption of the dimeric interface, because the IR absorption band for hydrogen bonding of carboxylate groups and solvent molecules is very sensitive to the hydrophobicity of its microenvironment (29). The major increase in IR absorption at 1619 cm^{-1} seen for both DsbC and DsbC-G49R at temperatures above 70°C indicates significant formation of protein aggregates.

To explore the biological significance of the results obtained in D_2O we further investigated the thermal stability of DsbC in buffer. Due to the Debye-Hückle dielectric effect (30) and the salting-in effect (24) on the IR absorbance, investigations of protein secondary structural changes have rarely been reported in buffer. We also find that the IR absorbance titration curve is no longer appropriate for analysis of structural change over a temperature range before protein aggregation (data not shown). Therefore, we propose a method for construction of the thermal titration curves in buffer by using the relative compositions of the major secondary

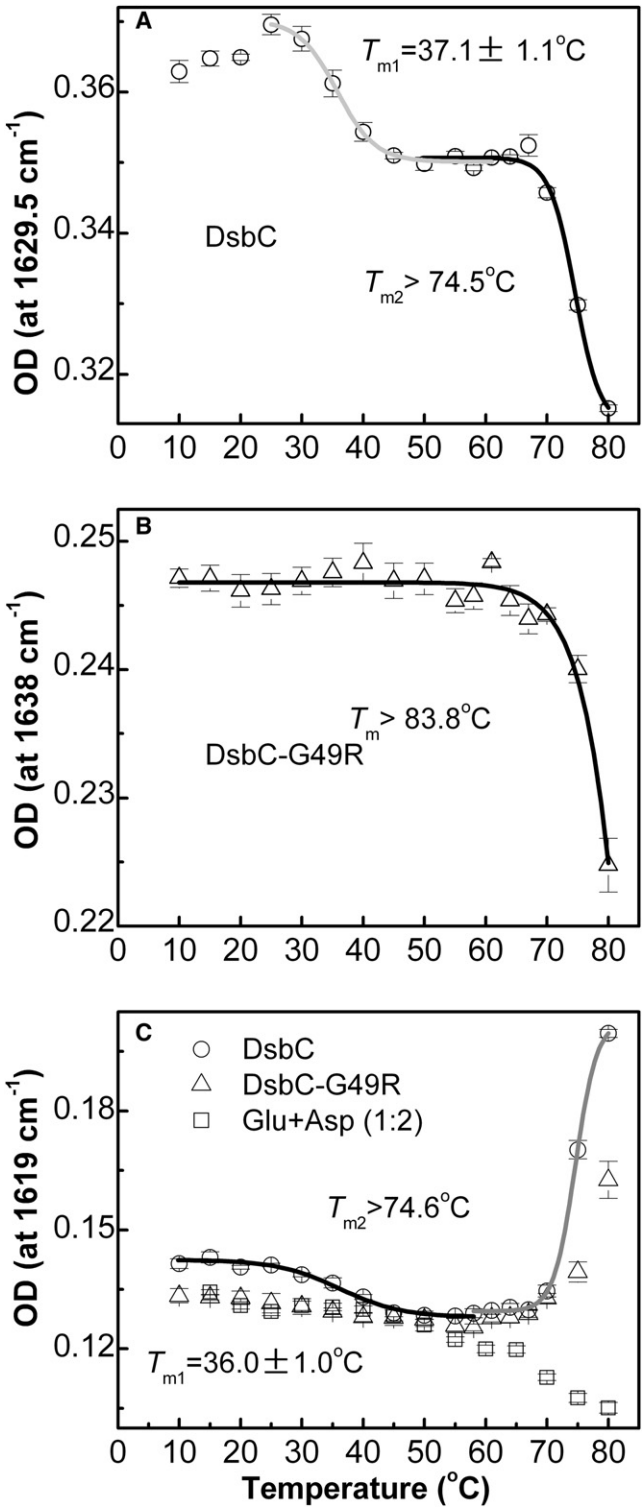

FIGURE 3 IR absorbance thermal titration curves in D_2O of (*A*) DsbC at 1629.5 cm^{-1}, and (*B*) DsbC-G49R at 1638 cm^{-1}. (*C*) Comparison of the thermal titration curves at 1619 cm^{-1} of DsbC, DsbC-G49R, and Glu/Asp in a weight ratio of 1:2 as in DsbC, with a total concentration of 12.5 mg/mL. The data are fitted to solid sigmoid curves with error bars expressed as mean ± SD ($n = 3$).

structural components instead of their IR absorption intensities. It is expected that the salt effect on the absolute IR absorption intensity can be leveled off by such an intrinsic scaling. The relative compositions were derived from the global multiple Gaussian-peak fitting of all the FTIR spectra acquired at different temperature with fixed peak positions, where total number of peaks for the global fitting is 7, i.e., 1614 and 1680 cm^{-1} both corresponding to anti-parallel β-sheets, 1633, 1643, and 1654 cm^{-1} to β-sheets, random coils and α-helix/loop respectively, 1660 and 1670 cm^{-1} both to turn.

We apply this method to construct the thermal titration curves of proteins in buffer. Fig. 4 presents the corresponding thermal titration curves for three major secondary structural components, i.e., β-sheets (1633 cm^{-1}), random coils (1643 cm^{-1}), and α-helix/loop (1654 cm^{-1}), respectively, for DsbC and DsbC-G49R. It is interesting to note that the percentages of the three secondary structural components in the monomer almost have the same value and do not change with the temperature before protein aggregation, if we consider the analytical uncertainty. This acts as an IR tag for the presence of the monomer. Inspecting the corresponding thermal titration curves for DsbC, we find that the three titration curves for the corresponding secondary structural compositions begin to converge to those of the DsbC-G49R monomer at the temperature of 40°C. This fact strongly suggests that the DsbC dimer begins to dissociate into monomers at a temperature above 40°C in buffer. Fitting the thermal titration curve of the random coils for DsbC leads to a T_m of 49.2 ± 0.7°C. This indicates that DsbC also dissociates in buffer but with a higher T_m, revealing a significant stabilizing effect of the buffer on the DsbC dimer.

T-jump time-resolved IR difference absorbance spectra

Fig. 5 displays the time-resolved IR difference absorbance spectra of DsbC and DsbC-G49R in response to the T-jump. We first focus on the absorption changes that take place around 1640 cm^{-1} (random coils), as we showed previously that one of the principal spectral differences occurs at this wavenumber. A striking difference between the T-jump time-resolved IR absorbance difference spectra of these two proteins is that DsbC has an absorption peak at 1640 cm^{-1} whereas DsbC-G49R shows a bleaching trough. The kinetics of absorption change for DsbC (Fig. 6 *C*) at this wavenumber is concentration-independent when we varied the protein concentration by a factor up to 3 (12.5, 6.25, and 3.12 mg/mL), and it can be resolved into two kinetic processes: an absorption phase with a time constant (τ) of 40 ± 10 ns, and a bleaching component with a τ of 150 ± 10 ns. The increase in absorption corresponds to a rapid but temporary increase in random coils for DsbC, suggesting disruption of the β-sheet at the dimeric interface leading to the formation of the geminate monomeric encounter pair, concomitant with the formation of random coils in the monomeric encounter pair. The bleaching of this newly formed random coil (77%) corresponds to the formation of the α-helical/loop structures at 1657 cm^{-1} (160 ± 10 ns, Fig. 6 *B*), a transition similar to that observed in DsbC-G49R where the bleaching at 1640 cm^{-1} occurs at the same time as the increase in absorption at 1658 cm^{-1}, both having a τ of 40 ± 10 ns (Fig. 6 *E*). Therefore, the absorption at 1640 cm^{-1} observed for DsbC strongly suggests the thermal-induced dimeric dissociation.

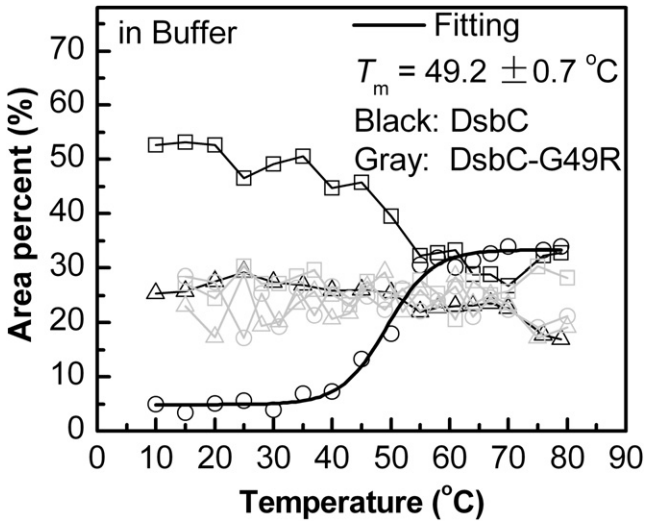

FIGURE 4 Thermal titration curves constructed by the relative compositions for three major secondary-structural components of DsbC and DsbC-G49R in phosphate buffer. β-sheets (□), α-helix/loop (△), and random coil (○). The thermal titration curve of random coils for DsbC is fitted as *bold solid curve*.

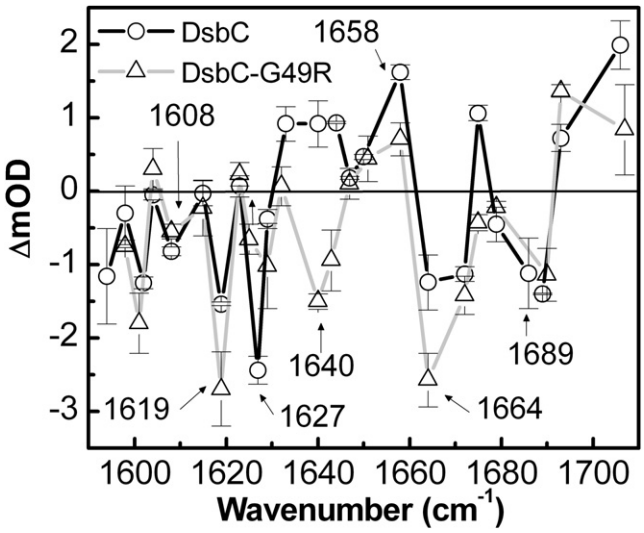

FIGURE 5 Time-resolved IR absorbance difference spectra in D_2O. The absorbance difference spectra in the amide I region were recorded at 1.4 μs after the T-jump from 28°C to 37.5°C for DsbC (○) and from 28°C to 35.5°C for DsbC-G49R (△). The data with error bars are expressed as mean ± SD ($n = 3$).

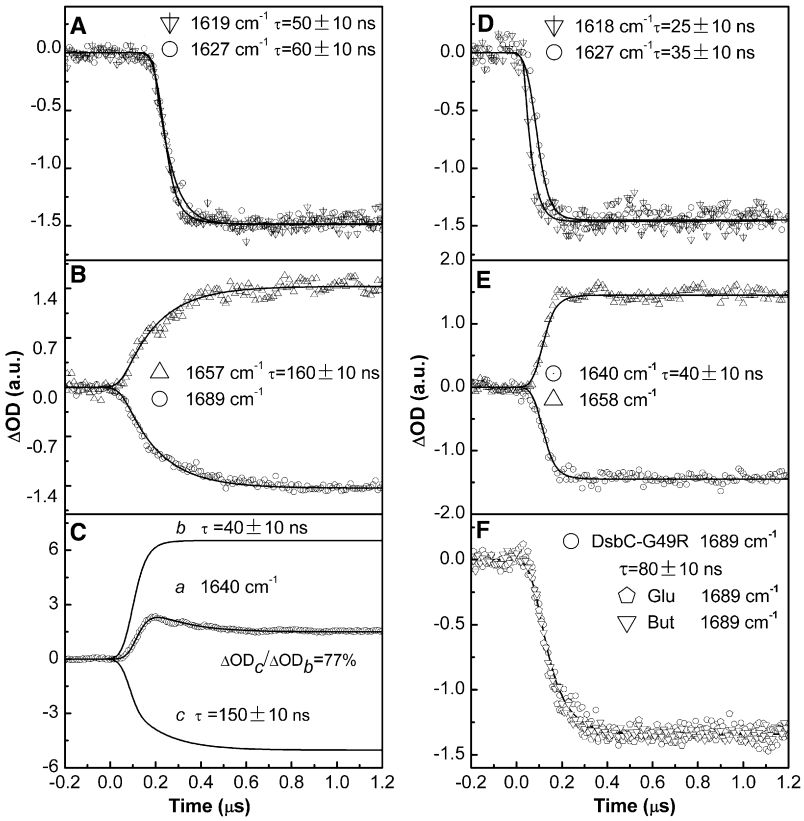

FIGURE 6 IR kinetic traces of DsbC and DsbC-G49R in D_2O. IR kinetic traces of (*A–C*) DsbC with a T-jump from 28°C to 37.5°C, and (*D–F*) of DsbC-G49R with a T-jump from 28°C to 35.5°C, were probed at different wavenumbers as indicated and fitted as solid curves by using a monoexponential function. In *C* the IR kinetic trace of DsbC at 1640 cm^{-1} (*a*) can be resolved into an absorption (*b*) and a bleaching curve (*c*) of a monoexponential process.

There are several other differences in the T-jump time-resolved IR difference absorbance spectra between DsbC and DsbC-G49R in Fig. 5. Their spectral assignments may be summarized as follows:

1. The 1608 cm^{-1} bleaching peak shows the thermal-induced breaking of intermolecular hydrogen bonds between the side-chain carboxylate of Glu or Asp and the amino groups.
2. Bleaching at the 1619 cm^{-1} peak originates from breaking of the hydrogen bond, as discussed in the previous section, and the corresponding kinetics are different for the dimer and monomer (Fig. 6, *A* and *D*).
3. The decrease in absorption at 1627 cm^{-1} (Fig. 6, *A* and *D*) corresponds to a decrease in β-sheet content. The amount of change is probably larger for the DsbC because a substantial amount of its β-sheets is involved in dimer formation that is likely to be disrupted by the temperature jump. Disruption of the β-sheet structures in DsbC-G49R indicates that partial disruption of the β-sheet structures of the building blocks of the thioredoxin fold also occurs on temperature jump.
4. DsbC and DsbC-G49R both exhibit a bleaching peak at 1664 cm^{-1}, indicating disruption of the turn structures in parallel with the disruption of the β-sheets.
5. The bleaching bands at ~1689 cm^{-1} (Fig. 6, *B* and *F*) for DsbC and DsbC-G49R mainly come from the thermal-induced bleaching of the side-chain carboxylic groups (−COOD) of residue Glu and Asp.

Fig. 6, *A* and *D*, show that the breaking of hydrogen bonds at 1619 cm^{-1} in DsbC-G49R is a faster process ($\tau \approx 25$ ns) than in DsbC ($\tau \approx 50$ ns), suggesting that the pertinent side-chain carboxyl groups in DsbC are located near the hydrophobic cleft, and the slower hydrogen bond breaking process reflects the thermal-induced opening of the cleft. The bleaching kinetics at 1627 cm^{-1} for DsbC (Fig. 6 *A*) and DsbC-G49R (Fig. 6 *D*) indicate disruption of the hydrogen bonds maintaining the β-sheet structures; here again the disruption process in DsbC is apparently slower than in DsbC-G49R, a trend similar to that for the kinetics at 1619 cm^{-1}.

Unlike the bleaching kinetics of DsbC-G49R probed at 1640 cm^{-1}, which well corresponds to that of the absorption band at 1658 cm^{-1}, the bleaching kinetics at 1689 cm^{-1} of DsbC-G49R with a τ of 80 ±10 ns (Fig. 6 *F*) does not match the kinetics of the other observable secondary structural components. We find that this type of kinetics is in agreement with the bleaching kinetics of Glu and butyric acid with a τ of 80 ± 10 ns (Fig. 6 *F*). Therefore, the kinetics in Fig. 6 *F* can be attributed to the thermal-induced proton dissociation from the carboxylic groups of the side-chain Glu and Asp rather than to anything that is specific to the protein backbone. Interestingly, the bleaching kinetics at 1689 cm^{-1} of DsbC assigned to the deprotonation of the side-chain carboxylic groups matches the kinetics at 1657 cm^{-1} (α-helix/loop, $\tau = 160 \pm 10$ ns) (Fig. 6 *B*). Because the deprotonation of the free carboxylic group in

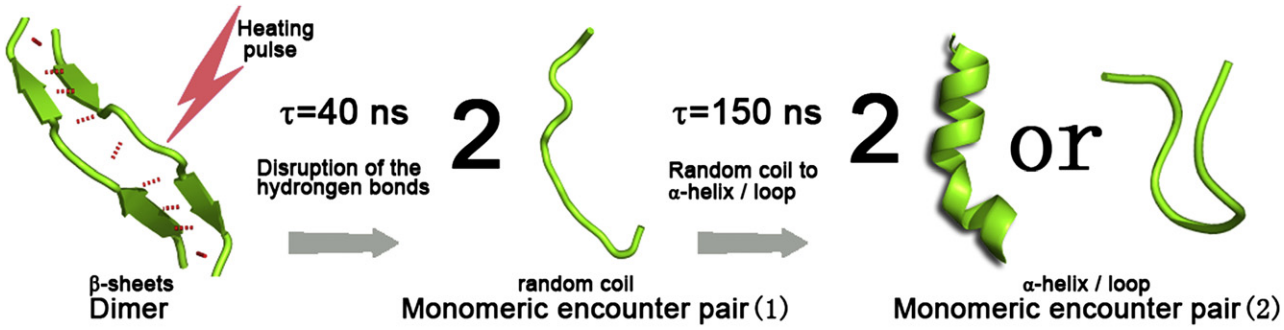

FIGURE 7 Model for thermal-induced two-stage dissociation/unfolding of DsbC at the dimeric interface.

solvent is a faster process (80 ns), the observed slower deprotonation can be attributed to those buried carboxylic groups where the opening of the hydrophobic cleft is the rate determining step.

The long-term kinetics were also investigated for temperature relaxation (cooling) processes over time intervals longer than several microseconds. The corresponding T-jump time-resolved IR absorbance difference spectra (with a delay time of up to ~50 μs) were found to be quite similar to those displayed in Fig. 5. We also plotted the CD titration curve of DsbC in buffer. The unfolding process in terms of the intensity loss at 222 nm can also be fitted by two two-state transitions with a T_m of 46.7 $\pm$ 0.3 and 74.0 $\pm$ 0.1°C, respectively. Due to the CD spectral overlap of the β-sheet and α-helical structures, the CD intensity change mainly reflects the thermal disruption of the β-sheet at the dimeric interface.

Based on the above facts as well as that the thermal-induced dissociation kinetics of dimeric DsbC are concentration-independent, indicative of a nondiffusion controlled process, we propose a two-stage scheme for the dissociation and unfolding of the DsbC (Fig. 7):

$$N_2 \leftrightarrow 2M \leftrightarrow 2U,$$

where N, M, and U refer to the native state, the intermediate germinate monomeric encounter pair, and the unfolded monomeric encounter pair, respectively. The first stage involves two synchronized processes: disruption of the intersubunit hydrogen bonds at the dimeric interface and concurrent formation of the random coil with a τ of 40 $\pm$ 10 ns leading to form the intermediate germinate monomeric encounter pair, immediately followed by a coil-helix/loop transition in the newly formed monomeric encounter pair with a τ of 160 $\pm$ 10 ns.

Biochemical evidence of DsbC dissociation

Size-exclusion chromatography (Fig. 8 *A*) shows that the elution volume of DsbC increases with increasing temperatures, but that of DsbC-G49R changes only slightly, close to that of DsbC at 65°C, indicating thermal-induced dissociation of DsbC at elevated temperatures. Moreover, nondenaturing PAGE (Fig. 8 *B*) of the mixture of DsbC and mmDsbC at an equal ratio in 100 mM K_2HPO_4/KH_2PO_4, pH 7.5, shows three bands: the upper band for native DsbC, the middle for the heterodimer, and the bottom for mmDsbC. The appearance of the heterodimer indicates the presence of dissociation of homodimers and reassociation of monomers. The subunit exchange reactions approach equilibrium within 10 min at 37°C, and even faster at 43°C, but there is very little within the timeframe of the experiment at 30°C. All these support the results obtained by IR spectroscopy.

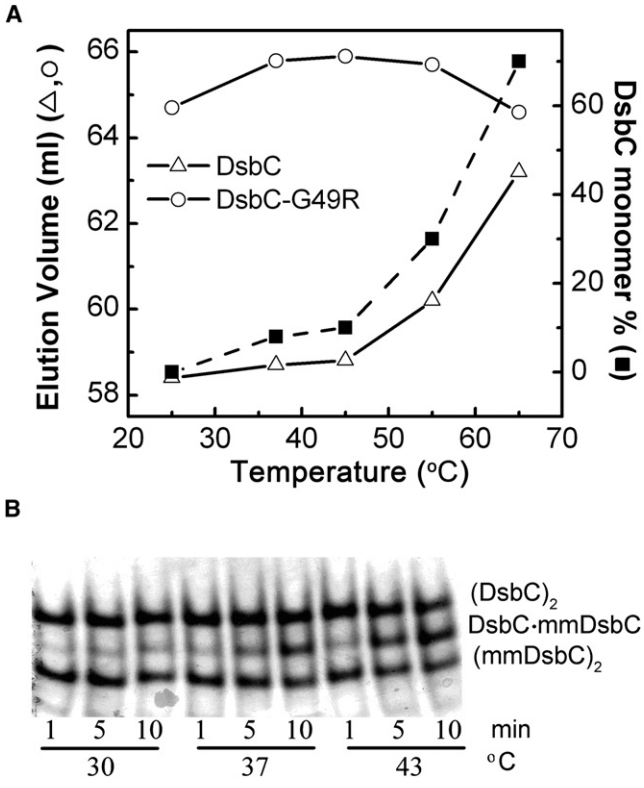

FIGURE 8 Biochemical evidence of DsbC dissociation. (*A*) Size-exclusion chromatography of DsbC and DsbC-G49R. Chromatography was carried out on a Superdex 75 water-jacketed column (Amersham, Biosciences, Piscataway, NJ) using 100 mM sodium phosphate buffer, pH 7.0, at 23°C, 37°C, 45°C, 55°C, and 65°C with a flow rate of 1 mL/min. (*B*) Nondenaturing 6% PAGE of hybrid mixtures. The mixtures of DsbC and mmDsbC at a ratio of 1:1 were incubated in buffer (100 mM K_2HPO_4/KH_2PO_4, pH 7.5) at 30°C, 37°C, and 43°C for 1, 5, and 10 min as indicated, and then mixed with a loading buffer in ice for electrophoresis.

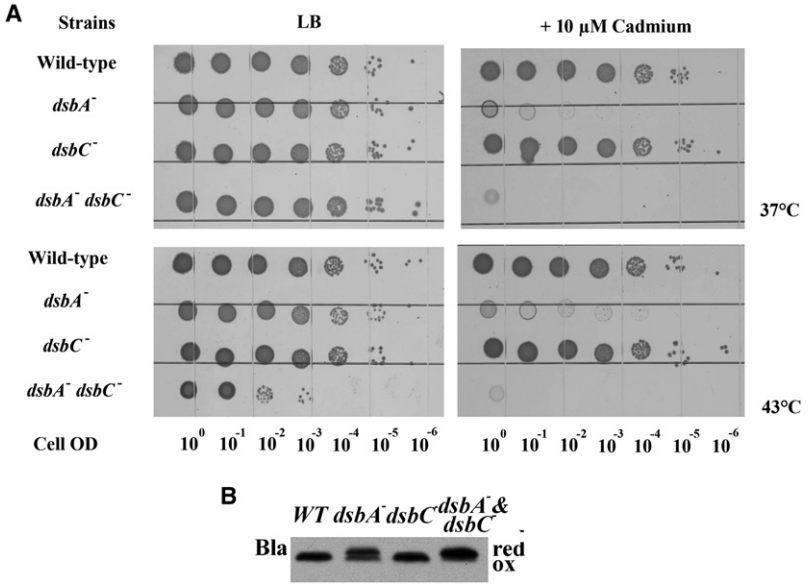

FIGURE 9 Potential oxidase activity of DsbC in vivo. (*A*) Spot titers for cadmium resistance. The *Escherichia coli* strain ER1821 with different genotypes shows various resistances to cadmium. Cells were grown on LB or LB with 10 μM cadmium at 37°C or 43°C as indicated in the figure. Wild-type and *dsbC*$^-$ strains show the highest cadmium resistance. The *dsbA*$^-$ *dsbC*$^-$ strain shows higher cadmium sensitivity than the *dsbA*$^-$ strain, and also shows 43°C temperature sensitivity to a certain extent. (*B*) Oxidation of Bla by DsbC in vivo red and ox represent reduced and oxidized Bla, respectively. All the experiments were carried out as described in the text.

The in vivo oxidase activity of DsbC

We next investigated the possible in vivo relevance of the apparent instability of the DsbC dimer. In the absence of the components of the disulfide catalytic machinery, periplasmic proteins contain multiple free thiols, and the binding of Cd^{2+} to these free thiols blocks disulfide bond formation, thus preventing proper folding of the proteins (31,32). Wild-type strains are much more cadmium-resistant (Cd^R), presumably because the free thiols are oxidized rapidly by the DsbA-DsbB disulfide bond formation machinery. Thus cadmium sensitivity is a good in vivo measure of thiol oxidase activity. Though DsbC is kept reduced by DsbD in the cell to function as an isomerase, Vertommen et al. (4) have shown that DsbC can function independent of DsbD, suggesting an oxidase role in vivo. In consistency with their results, we found that the *dsbA*$^-$ *dsbC*$^-$ strain does show increased cadmium sensitivity compared with the *dsbA*$^-$ strain, indicating a weak in vivo oxidase activity of DsbC (Fig. 9 *A*). To directly measure the in vivo oxidase activity of DsbC, we further examined the oxidation state of TEM1-Bla, which contains only a single disulfide bond and is active even in the absence of this disulfide bond. The formation of this disulfide requires an oxidase but not an isomerase. Thus the state of oxidation of Bla is a good measure of oxidase activity in vivo. As shown in Fig. 9 *B*, Bla is mostly oxidized in the wild-type and *dsbC*$^-$ strains, but largely reduced with a small portion oxidized in the *dsbA*$^-$ strain. In the *dsbA*$^-$*dsbC*$^-$ strain the oxidized portion is almost absent. These data strongly indicate that DsbC is able to function as an oxidase in vivo.

We reported previously that monomeric thioredoxin-like proteins or domains, which have only oxidase or reductase activity, can form dimers and acquire new isomerase activity when fused with an association component, such as the N-terminal domain of DsbC (2) or the bacterial proline *cis*/*trans* isomerase FkpA (33), and accordingly proposed a strategy by which biological molecules could gain new functions and achieve higher efficiency through an evolution process. The thermal instability of DsbC investigated in this study by temperature-dependent FTIR and T-jump time-resolved IR absorbance difference spectroscopy in D_2O and buffer as well, together with the in vitro and in vivo biological determinations, is just an imprint of such an evolution.

In addition, it has been pointed out recently that DsbC is not restricted to function only as an isomerase in the isomerization pathway, but is able to function in both the oxidation and isomerization pathways, and may possibly act as a stand-alone protein folding catalyst (4). The thermal instability of DsbC characterized in this study provides what we believe to be is an appropriate structural base and evolutional significance for this new viewpoint.

SUPPORTING MATERIAL

Materials, methods, and a table are available at http://www.biophysj.org/biophysj/supplemental/S0006-3495(09)01441-6.

We thank Dr. James Bardwell in the Howard Hughes Medical Institute, Department of Molecular, Cellular, and Developmental Biology, University of Michigan, for very helpful discussions. We thank Dr. Ling-An Wu in the Institute of Physics, Chinese Academy of Sciences, for final proofreading of the writing.

This work was supported by the Chinese Ministry of Science and Technology (2006CB910903, 2006CB806508), the China National Science Foundation (30620130109), and Chinese Academy of Sciences Innovative Project (KJCX2-SW-w29).

REFERENCES

1. Nakamoto, H., and J. C. Bardwell. 2004. Catalysis of disulfide bond formation and isomerization in the Escherichia coli periplasm. *Biochim. Biophys. Acta.* 1694:111–119.
2. Zapun, A., D. Missiakas, S. Raina, and T. E. Creighton. 1995. Structural and functional characterization of DsbC, a protein involved in

disulfide bond formation in Escherichia coli. *Biochemistry.* 34: 5075–5089.

3. Chen, J., J. L. Song, S. Zhang, Y. Wang, D. F. Cui, et al. 1999. Chaperone activity of DsbC. *J. Biol. Chem.* 274:19601–19605.
4. Vertommen, D., M. Depuydt, J. Pan, P. Leverrier, L. Knoops, et al. 2008. The disulphide isomerase DsbC cooperates with the oxidase DsbA in a DsbD-independent manner. *Mol. Microbiol.* 67:336–349.
5. McCarthy, A. A., P. W. Haebel, A. Torronen, V. Rybin, E. N. Baker, et al. 2000. Crystal structure of the protein disulfide bond isomerase, DsbC, from Escherichia coli. *Nat. Struct. Biol.* 7:196–199.
6. Zhao, Z., Y. Peng, S. F. Hao, Z. H. Zeng, and C. C. Wang. 2003. Dimerization by domain hybridization bestows chaperone and isomerase activities. *J. Biol. Chem.* 278:43292–43298.
7. Bader, M. W., A. Hiniker, J. Regeimbal, D. Goldstone, P. W. Haebel, et al. 2001. Turning a disulfide isomerase into an oxidase: DsbC mutants that imitate DsbA. *EMBO J.* 20:1555–1562.
8. Ke, H., S. Zhang, J. Li, G. J. Howlett, and C. C. Wang. 2006. Folding of Escherichia coli DsbC: characterization of a monomeric folding intermediate. *Biochemistry.* 45:15100–15110.
9. Pan, J. L., I. Sliskovic, and J. C. Bardwell. 2008. Mutants in DsbB that appear to redirect oxidation through the disulfide isomerization pathway. *J. Mol. Biol.* 377:1433–1442.
10. Inaba, K., S. Murakami, M. Suzuki, A. Nakagawa, E. Yamashita, et al. 2006. Crystal structure of the DsbB-DsbA complex reveals a mechanism of disulfide bond generation. *Cell.* 127:789–801.
11. Phillips, C. M., Y. Mizutani, and R. M. Hochstrasser. 1995. Ultrafast thermally induced unfolding of RNase A. *Proc. Natl. Acad. Sci. USA.* 92:7292–7296.
12. Surewicz, W. K., and H. H. Mantsch. 1988. New insight into protein secondary structure from resolution-enhanced infrared spectra. *Biochim. Biophys. Acta.* 952:115–130.
13. Arrondo, J. L., A. Muga, J. Castresana, and F. M. Goni. 1993. Quantitative studies of the structure of proteins in solution by Fourier-transform infrared spectroscopy. *Prog. Biophys. Mol. Biol.* 59:23–56.
14. Leeson, D. T., F. Gai, H. M. Rodriguez, L. M. Gregoret, and R. B. Dyer. 2000. Protein folding and unfolding on a complex energy landscape. *Proc. Natl. Acad. Sci. USA.* 97:2527–2532.
15. Dyer, R. B., F. Gai, W. H. Woodruff, R. Gilmanshin, and R. H. Callender. 1998. Infrared Studies of Fast Events in Protein Folding. *Acc. Chem. Res.* 31:709–716.
16. Callender, R., and R. B. Dyer. 2006. Advances in time-resolved approaches to characterize the dynamical nature of enzymatic catalysis. *Chem. Rev.* 106:3031–3042.
17. Ye, M. P., Q. L. Zhang, H. Li, Y. X. Weng, W. C. Wang, et al. 2007. Infrared spectroscopic discrimination between the loop and alpha-helices and determination of the loop diffusion kinetics by temperature-jump time-resolved infrared spectroscopy for cytochrome *c*. *Biophys. J.* 93:2756–2766.
18. Zhang, Q. L., L. Wang, Y. X. Weng, X. G. Qiu, W. C. Wang, et al. 2005. Nanosecond-time-resolved infrared spectroscopic study of fast relaxation kinetics of protein folding by means of laser-induced temperature-jump. *Chin. Phys.* 14:2484–2490.
19. Wang, T., Y. Zhu, Z. Getahun, D. Du, C. Y. Huang, et al. 2004. Length Dependent Helix-Coil Transition Kinetics of Nine Alanine-Based Peptides. *J. Phys. Chem. B.* 108:15301–15310.
20. Huang, C. Y., Z. Getahun, Y. Zhu, J. W. Klemke, W. F. DeGrado, et al. 2002. Helix formation via conformation diffusion search. *Proc. Natl. Acad. Sci. USA.* 99:2788–2793.
21. Huang, C. Y., J. W. Klemke, Z. Getahun, W. F. DeGrado, and F. Gai. 2001. Temperature-dependent helix-coil transition of an alanine based peptide. *J. Am. Chem. Soc.* 123:9235–9238.
22. Williams, S., T. P. Causgrove, R. Gilmanshin, K. S. Fang, R. H. Callender, et al. 1996. Fast events in protein folding: Helix melting and formation in a small peptide. *Biochemistry.* 35:691–697.
23. Quan, S., I. Schneider, J. Pan, A. Von Hacht, and J. C. Bardwell. 2007. The CXXC motif is more than a redox rheostat. *J. Biol. Chem.* 282:28823–28833.
24. Zangi, R., M. Hagen, and B. J. Berne. 2007. Effect of ions on the hydrophobic interaction between two plates. *J. Am. Chem. Soc.* 129:4678–4686.
25. Onsager, L. 1936. Electric moments of molecules in liquids. *J. Am. Chem. Soc.* 58:1486–1493.
26. Susi, H., and D. M. Byler. 1983. Protein-Structure by Fourier-Transform Infrared-Spectroscopy - 2ND Derivative Spectra. *Biochem. Biophys. Res. Commun.* 115:391–397.
27. Susi, H., and D. M. Byler. 1986. Resolution-enhanced Fourier transform infrared spectroscopy of enzymes. *Methods Enzymol.* 130:290–311.
28. Ye, M. P., L. Heng, Q.-L. Zhang, Y.-X. Weng, and X.-G. Qiu. 2007. Intermolecular hydrogen bonds formed between amino acid molecules in aqueous solution investigated by temperature-jump nanosecond time-resolved transient mid-IR spectroscopy. *Chin. J. Chem. Phys.* 20:461–467.
29. Wright, W. W., M. Laberge, and J. M. Vanderkooi. 1997. Surface of cytochrome *c*: infrared spectroscopy of carboxyl groups. *Biochemistry.* 36:14724–14732.
30. Kumar, S., and R. Nussinov. 1999. Salt bridge stability in monomeric proteins. *J. Mol. Biol.* 293:1241–1255.
31. Rensing, C., B. Mitra, and B. P. Rosen. 1997. Insertional inactivation of dsbA produces sensitivity to cadmium and zinc in *Escherichia coli*. *J. Bacteriol.* 179:2769–2771.
32. Stafford, S. J., D. P. Humphreys, and P. A. Lund. 1999. Mutations in dsbA and dsbB, but not dsbC, lead to an enhanced sensitivity of *Escherichia coli* to Hg^{2+} and Cd^{2+}. *FEMS Microbiol. Lett.* 174:179–184.
33. Arredondo, S., L. Segatori, H. F. Gilbert, and G. Georgiou. 2008. De novo design and evolution of artificial disulfide isomerase enzymes analogous to the bacterial DsbC. *J. Biol. Chem.* 283:31469–31476.
34. Barth, A. 2007. Infrared spectroscopy of proteins. *Biochim. Biophys. Acta.* 1767:1073–1101.
35. Mukherjee, S., P. Chowdhury, and F. Gai. 2007. Infrared study of the effect of hydration on the Amide I band and aggregation properties of helical peptides. *J. Phys. Chem. B.* 111:4596–4602.
36. van Stokkum, I. H. M., H. Linsdell, J. M. Hadden, P. I. Haris, D. Chapman, et al. 1995. Temperature-induced changes in protein structures studied by Fourier transform infrared spectroscopy and global analysis. *Biochemistry.* 34:10508–10518.
37. Timasheff, S. N., H. Susi, and L. Stevens. 1967. Infrared spectra and protein conformations in aqueous solutions. II. Survey of globular proteins. *J. Biol. Chem.* 242:5467–5473.
38. Kubelka, J., and T. A. Keiderling. 2001. Differentiation of β-sheet-forming structures: ab initio-based simulations of IR absorption and vibrational CD for model peptide and protein β-sheets. *J. Am. Chem. Soc.* 123:12048–12058.
39. Jackson, M., and H. H. Mantsch. 1995. The use and misuse of FTIR spectroscopy in the determination of protein structure. *Crit. Rev. Biochem. Mol. Biol.* 30:95–120.
40. Filosa, A., Y. Wang, A. A. Ismail, and A. M. English. 2001. Two-dimensional infrared correlation spectroscopy as a probe of sequential events in the thermal unfolding of cytochromes *c*. *Biochemistry.* 40:8256–8263.
41. Wilder, C. L., A. D. Friedrich, R. O. Potts, G. O. Daumy, and M. L. Francoeur. 1992. Secondary structural analysis of two recombinant murine proteins, interleukins 1 alpha and 1 beta: is infrared spectroscopy sufficient to assign structure. *Biochemistry.* 31:27–31.
42. Zhao, X. Y., F. S. Chen, W. T. Xue, and L. Lee. 2008. FTIR spectra studies on the secondary structures of 7S and 11S globulins from soybean proteins using AOT reverse micellar extraction. *Food Hydrocoll.* 22:568–575.
43. Bandekar, J., and S. Krimm. 1980. Vibrational analysis of peptides, polypeptides, and proteins. VI. Assignment of beta-turn modes in insulin and other proteins. *Biopolymers.* 19:31–36.
44. Dong, A., P. Huang, and W. S. Caughey. 1990. Protein secondary structures in water from 2ND-derivative Amide-I infrared-spectra. *Biochemistry.* 29:3303–3308.